applied sciences

MDPI

Article

Model Tests on Jacked Pile Penetration Characteristics Considering a Static Press-in Piling Machine

Yinan Li, Rongyue Zheng * and Yuebao Deng

College of Civil Engineering and Geographical Environment, Ningbo University, Ningbo 315211, China; 2211110074@nbu.edu.cn (Y.L.); dengyuebao@nbu.edu.cn (Y.D.)
* Correspondence: rongyue@nbu.edu.cn; Tel.: +86-13626747949

Abstract: This study incorporates a static press-in piling machine into the conventional laboratory model tests for jacked piles. By conducting a comparative analysis between two tests, one involving the static press-in piling machine and the other focusing solely on pile jacking, this study aims to unveil the variations in penetration characteristics with pile sinking depth during the process of pile jacking under the constraint imposed by the static press-in piling machine. When considering the impact of the piling machine, the pile pressing force, pile sinking resistance, pile axial force, and unit side friction resistance of the pile body are higher compared to test results that only focus on pile jacking. There is an acceleration in the total side friction resistance within the depth range of 20 to 30 cm. Additionally, the reduction rate of axial force during the entire pile jacking process is 2% higher, with a general reduction in the "side resistance degradation" phenomenon. The soil pressure around the pile exhibits an initial increase followed by a decrease. The authors believe that the model box test of the jacked pile, considering the pile machine, would be more aligned with engineering practice.

Keywords: jacked pile; static press-in piling machine; penetration characteristics; model tests

Citation: Li, Y.; Zheng, R.; Deng, Y. Model Tests on Jacked Pile Penetration Characteristics Considering a Static Press-in Piling Machine. *Appl. Sci.* **2024**, *14*, 1985. https://doi.org/10.3390/app14051985

Academic Editor: Tiago Miranda

Received: 27 January 2024
Revised: 20 February 2024
Accepted: 23 February 2024
Published: 28 February 2024

1. Introduction

With the increasing advancement of jacked pile technology and the rapid development of pile machinery, jacked pile is widely used in soft soil areas. In order to meet various construction conditions, the weight of the static press-in piling machine is increasing, leading to frequent accidents during the pile jacking process. Hence, it is imperative not to overlook the impact of the piling machine on the pile penetration characteristics and soil squeezing effect during construction. Effective estimation of pile jacking resistance before pile foundation construction is essential for guiding the selection of static press-in piling machines, improving jacked pile techniques, and ultimately making the pile jacking process go smoothly [1–5].

A substantial number of scholars have conducted various studies on the penetration characteristics of piles. In field tests, Doherty and Gavin [6] studied the penetration characteristics of jacked piles in layered cohesive soil and examined how different pile jacking methods affect the development and alteration of pile side friction resistance. Kou et al. [7] measured the strain distribution of the pile body and evaluated the influence of the pile depth and soil resistance on the axial force and lateral friction resistance of the pile body through the strain distribution. Some scholars have studied the different mechanical characteristics of the open and closed PHC pipe piles through field tests and revealed the distribution law of soil pressure at the pile–soil interface [8–10]. In terms of numerical simulation, Ding et al. [11] conducted a friction analysis on the penetration process of large diameter steel using the discrete element method (DEM) and studied the impact of the contact parameters on side friction. Jin et al. [12] used the numerical platform to establish the nonlinear relationship between pile resistance and sand density to guide the

reasonable design of a pile foundation in sand. Zhou et al. [13] independently developed a noncircular particle numerical simulation program to analyze the interaction between soil and piles during pile penetration in sand. Zhang et al. [14] proposed the displacement penetration method, which uses the boundary displacement condition to facilitate pile penetration, rendering it more in line with the actual situation of pile jacking. It can be seen that a series of field tests and numerical simulation research studies have been carried out to study the pile penetration characteristics. However, neither of them has taken into account the influence of the static press-in piling machine on the research results, making them not entirely suitable for engineering practice.

The model test is of low cost and fleeting period, prompting many scholars to study the problem of pile jacking through model tests. Abendroth and Greimann [15] obtained the stress characteristics of piles in sand with different compactness through the model box test of steel pipe piles. Altaee et al. [16] analyzed the critical depth of pile end resistance in the model pile test. Lehane and Gavin [17] studied the influence of soil stress, diameter, and wall thickness on the characteristics of pipe pile jacking in sand by a test. It can be found that many studies on the penetration mechanism of jacked piles have focused on sand soil. However, viscous soil can more accurately replicate the actual engineering conditions of jacked piles in coastal soft areas [18]. Hence, investigating the penetration characteristics of jacked piles in soft clay soil through model tests is meaningful.

Through many traditional pile jacking model tests, scholars have acquired the variation law of pile end resistance, pile side resistance, and pile jacking force in the process of pile pressing in different foundation soils and proposed the phenomenon of "side resistance degradation" to correct the results and finally summed up the relevant laws about the penetration characteristics of jacked pile [19–22]. Based on the above research and analysis, it can be concluded that, in the past, research on jacked piles was mostly limited to the piles themselves, rather than to considering the constraints of the surrounding environment. In actual construction, the process of pile jacking will inevitably be affected by surface constraints such as the static press-in piling machine and surrounding roads. However, the surrounding environmental constraints involved in the scholars' research differ, and the research content is not systematically conducted. Lu et al. [23] investigated the importance of static press-in piling machine constraints through field tests and numerical simulations. Wang and Wei [24] studied the squeezing effect of road-constrained sinking piles by use of numerical simulations. Therefore, building upon the foundation of model testing, this paper places the static press-in piling machine at the center of attention. Model box tests incorporating the piling machine have been devised and compared with traditional model tests. The study's primary focus is the piling machine's influence on the penetration characteristics of jacked piles.

With the effect of the static press-in piling machine as the main condition, the penetration characteristics, pile-soil interface friction characteristics, and soil disturbance characteristics of jacked piles in soft clay in the Ningbo area are studied through a self-designed model test considering the piling machine, establishing the theory of static pressure piling rig–pile–site soil layer synergistic fusion.

2. Model Test

2.1. Soil Samples

The soil samples were extracted from a foundation pit project in Yinzhou District, Ningbo City, Zhejiang Province, China, at a depth of 3–4 m below the surface. It is a typical saturated soft clay commonly encountered in the Ningbo region. This soil layer is characterized by its weakness, flowing plastic state, and thick layering, displaying high compressibility and moisture content.

2.2. Testing Equipment

The model test system, which considers the impact of the static press-in piling machine, primarily consists of the model test platform, the data acquisition system, the model pile, and the long leader models of the piling machine.

The pile foundation model test platform comprises a self-designed loading system and a model box which is manufactured by Shanghai Zhubang Measurement and Control Technology Co., Ltd. in Shanghai, China. The loading system consists of a reaction frame, a power device, and three jacks. The reaction frame's overall structure comprises a base, two side reaction frames, and an intermediate reaction frame. The base measures 2.5 m in length, 1.9 m in width, and 0.2 m in height. The two side reaction frames are 2.5 m tall with a span of 1.9 m. The central reaction frame, standing at 2.8 m high, is constructed with a self-designed adjustable steel plate secured by four long anchor bolts. The jacks on both sides simulate the loading of the piling machine, while the middle jack is utilized for pile jacking. The model box is constructed from welded steel plates and measures 2 m × 1.2 m × 1.2 m (length × width × height, respectively), as illustrated in Figure 1.

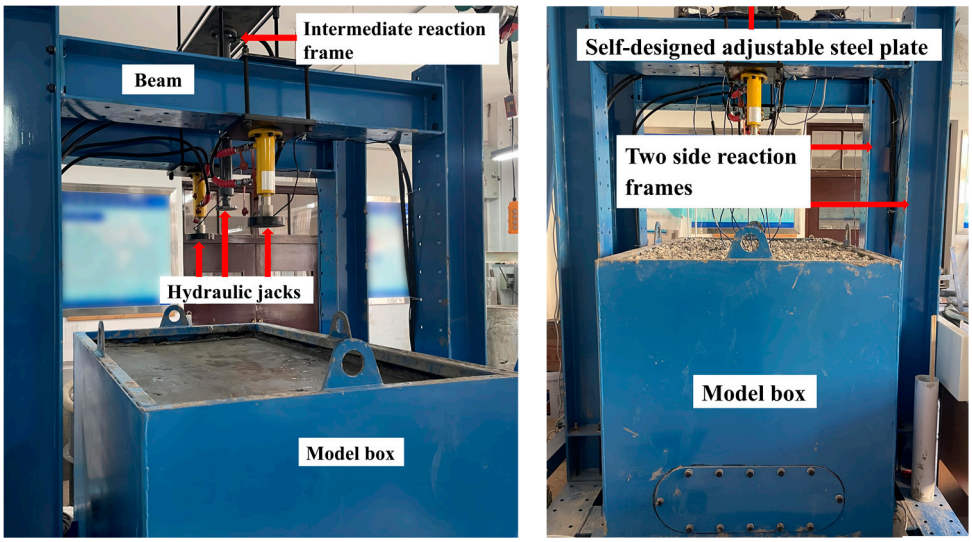

Figure 1. Pile foundation model test platform diagram. (**a**) Platform detail diagram. (**b**) Overall platform diagram.

In accordance with the geometric similarity theory, the selection of the static press-in piling machine is scaled down in proportion to the actual project. The prefabricated long leader models of the piling machine measure 1 m × 0.15 m × 0.1 m (length × width × height, respectively), with a 0.6 cm distance between the long leaders. The combined load applied by each group of hydraulic jacks and the dead weight of the long leader model of the pile machine amounts to 0.68 t. Through the application of load and the grounding area of the long leader, the specific pressure of the long leader grounding is determined to be 45 kPa. Additionally, a 1 cm thick steel plate is placed under the concrete model to simulate the real contact between the static press-in piling machine and the ground. Figure 2 depicts the schematic diagram of the actual project and the model test of the jacked pile machine.

The model pile is a solid cylindrical precast concrete pile. Given the boundary effect of pile jacking, the radial range of pile jacking in clay extends approximately 5 times the diameter of the pile away from the pile body. Based on the dimensions of the model box, the pile diameter is determined as D =100 mm and the length as L = 600 mm. The strain gauge grooves are reserved on the pile side, and the strain gauges are adhered to the groove of the low-strength solid model pile using the groove method. A total of 14 strain gauges were positioned on the model pile, with 7 on each side. Strain gauges with a base length of 4 mm were placed at the pile end and top, while strain gauges with a base length of 10 mm

were positioned at other locations to enhance the precision of the measurement results. The surfaces of the strain gauges are coated with silica gel, and epoxy resin is used to seal the grooves before polishing the epoxy resin surface with sandpaper, in order to reproduce the pile–soil interaction as accurately as possible. Figure 3 depicts the layout diagram of the strain gauges. Following this, the groove is sealed with epoxy resin and polished to form a pile.

(**a**) (**b**)

Figure 2. Schematic diagram of long leader for piling machine. (**a**) Piling machine in practical engineering. (**b**) Piling machine in model test.

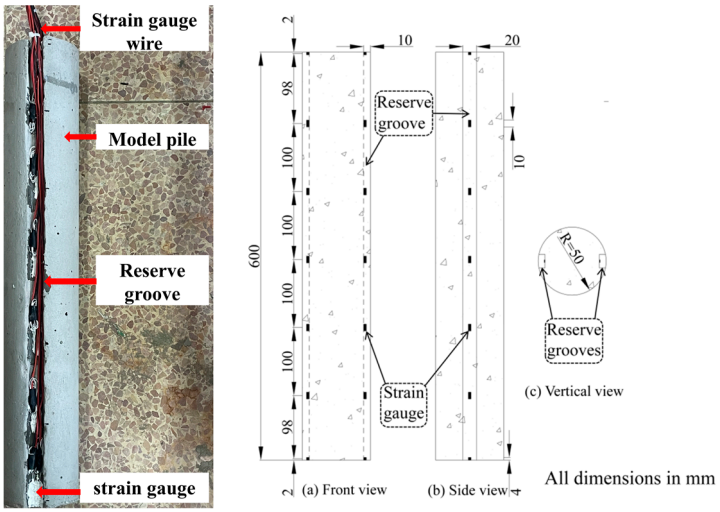

(**a**) (**b**)

Figure 3. Layout diagram of strain gauges. (**a**) Model Pile. (**b**) Three views of the model pile.

The data acquisition system primarily utilizes the DH3816N static strain acquisition instrument which is manufactured by Donghua Testing Technology Co., Ltd. in Jiangsu, China and wireless earth pressure gauge manufactured by AVIC zhonghang Electronic Measuring Instruments Co., Ltd. in Shijiazhuang, China for collecting pertinent data.

2.3. Test Scheme

There are two sets of model tests designed. Test PS1 focuses solely on the pile jacking, while test PS2 considers the pile jacking under the influence of the static press-in piling machine. The test controls the pile jacking rate at 1 mm/s, as shown in Table 1.

Table 1. Test scheme.

Test Number	Pile Length (mm)	Pile Diameter (mm)	Pile Driving Speed (mm/s)	Longitudinal Spacing between Long Leaders (mm)	Vertical Load of the Static Press-in Piling Machine (kPa)
PS 1	600	100	1		
PS 2	600	100	1	600	45

2.4. Test Process

2.4.1. Model Foundation Soil

Prior to soil filling, a 5 cm thick layer of polyurethane foam was placed inside the model box to minimize the boundary effects of the experiment.

After the soil samples from the foundation pit project in the Ningbo area are sent to the laboratory, they are filled into the trench in four separate times by using the layered filling method to ensure that the filling height of the last layer of soil is controlled at 1.1 m. During the process of layered filling soil samples, after each layer is filled, the soil is compacted by a small tamping machine. Subsequently, the soil is covered with a plastic film, and boards are placed on its surface. Weight is stacked on the board for one day to ensure even compaction of the soil samples in each layer to meet the test requirements. After the soil sample is even, an appropriate amount of water is sprayed on its surface to ensure the uniformity of the test soil sample's moisture. Subsequently, a preloading load of 10 kPa is continuously applied to the foundation soil for 14 days in each test, and an impervious plastic film is used to seal the surface of the foundation soil of the model box to prevent water loss. The PS2 test considers the influence of the static press-in piling machine. Because the piling machine is susceptible to jacking in the soft foundation soil of the coastal area [25], the soil replacement cushion method is commonly employed to enhance the foundation's bearing capacity. To align with engineering practice, a 0.1 m thick gravel cushion is uniformly laid on the model box soil and compacted to meet the foundation's bearing capacity requirements after preloading, After the gravel layer is compacted, the soil stands for about 20 days to reach a stable state. Subsequently, a series of soil mechanics laboratory tests, in accordance with the 'Standard for Geotechnical Test Methods' (GB/T50123-2019) [26], is carried out to determine the physical and mechanical parameters of the soil samples obtained from the model box foundation soil. The soils are separately prepared for each test, and all soil tests are conducted using samples from the same batch, prepared in strict accordance with the same re-preparation process. Following preparation, a series of soil mechanics laboratory tests are carried out to ensure that the physical and mechanical properties of the two groups of experimental soils are essentially identical. The fundamental physical properties of the model box foundation soil are presented in Table 2.

Table 2. Physical properties index of model box foundation soil.

Density ρ (kg/m^3)	Severe Γ (kN/m^3)	Moisture Content W (%)	Liquid Limit w_L (%)	Plastic Limit w_P (%)	Cohesion c (kPa)	Internal Friction Angle φ (°)	Compression Modulus E_{s1-2} (MPa)
1730	16.84	35	34.8	21.2	14.4	8.6	2.54

In the assessment of the uniformity of the model foundation soil, soil samples were extracted at foundation soil depths of 0.1 m, 0.3 m, and 0.5 m, as well as from the surface of the foundation soil using a Luoyang shovel and a ring knife. Subsequently, physical and mechanical tests were conducted. The results indicated that the water content and mechanical properties of the soil samples were relatively similar, suggesting a relatively uniform model foundation soil. Figure 4 displays some of the instruments used in the measurement process.

(**a**) (**b**)

Figure 4. Instruments used in the measurement process. (**a**) STHX-4A electric hot blast dryer. (**b**) Consolidation apparatus. (All manufactured by Zhejiang Geotechnical Instrument Manufacturing Co., Ltd. in Shaoxing, China).

2.4.2. Sensor Layout

The resistance strain gauges have already been embedded in the pile. To measure the variation in soil pressure around the pile, two soil pressure gauges (A1 and A2) are positioned at distances of 1 times the pile diameter (100 mm) from the expected pile jacking position, at soil depths of 150 mm and 350 mm, respectively, and another two soil pressure gauges (A3 and A4) are placed at distances of 2 times the pile diameter (200 mm) and 3 times the pile diameter (300 mm), respectively, at a soil depth of 350 mm. Figure 5 provides a comparison between the actual project and the model test.

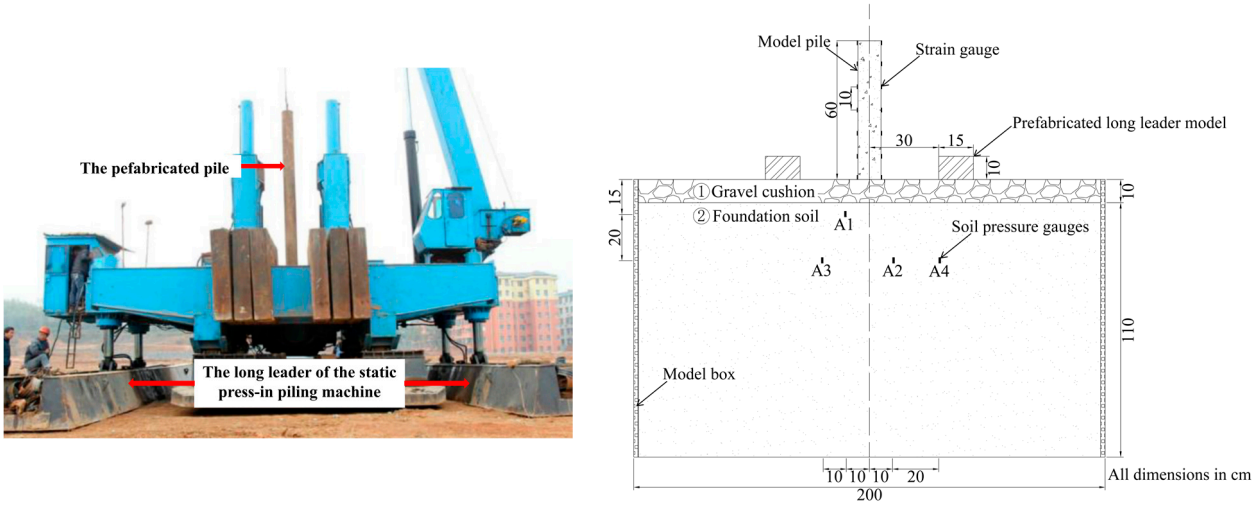

(**a**) (**b**)

Figure 5. Comparison between actual project and model test. (**a**) The actual project. (**b**) The model test.

2.4.3. Experimental Scheme

Test PS1 only considers the pile jacking at a speed of 1 mm/s. Test PS2 considers the pile jacking under the influence of the static press-in piling machine. This paper only considers a pile penetration depth of 60 cm, so the pile jacking pressure is much smaller compared to the load of the piling machine. Therefore, in test PS2, it is assumed that the pile jacking pressure does not impact the total weight of the piling machine, and the vertical load of the piling machine is directly provided by two jacks on either side. The prefabricated long leader model's edge is positioned 30 cm away from the pile shaft, with

a ground pressure of 45 kPa. When the value of the pressure sensor is stabilized, the pile jacks at the same speed.

3. Test Results and Analysis

3.1. Test Data Processing and Analysis

The processing of data from the static strain acquisition instrument is the main component of the test data processing, and it requires calculation. The remaining data can be directly obtained from the pile top pressure sensor and the wireless earth pressure gauge. For the analysis of the experimental data, the causes of various phenomena in the experimental process are mainly explained based on the "adhesion-plough" theory proposed from the perspective of tribology [27].

3.1.1. Pile Axial Force Calculation

The average strain ε_i of each section is obtained by the static strain acquisition instrument, and the axial force Ni of the pile during the pile jacking process can be obtained according to Formula (1).

$$N_i = E_S \varepsilon_i A_S \quad (1)$$

where N_i is the axial force of the pile at the i-th section, E_S is the elastic modulus of the pile, ε_i is the strain change value measured by the strain gauge at the i-th section, and A_S is the cross-sectional area of the pile.

3.1.2. Pile End Resistance and Pile Side Friction Resistance Calculation

Pile end resistance and the pile side friction resistance can be calculated using Formulas (2)–(4).

$$Q_i = N_i - N_{i+1} \quad (2)$$

$$q_i = \frac{Q_i}{A_b} = \frac{N_i - N_{i+1}}{2\pi r L_i} \quad (3)$$

where Q_i is the side friction resistance of the i-th section pile; q_i is the unit side friction resistance of the pile body of the i-th section; A_b is the pile side surface area from section i to section i + 1; r is the radius of the pile; L_i is the distance between the i + 1 section and the i + 1 section.

$$q_t = \frac{Q_t}{A_t} \quad (4)$$

where q_t is the end resistance of jacked pile; Q_t is the axial force at the pile end; A_t is the flat cross-sectional area of the pile end.

3.1.3. Theoretical Introduction

According to the classical tribology theory, the sliding friction is the sum of the adhesion and plough effect. The "adhesion-plough" theory was first proposed and used in the friction between metal surfaces [28,29], while this paper applies the theory to the pile–soil interface to analyze the experimental results. In the process of pile jacking, the soil body is subjected to the pile body's ploughing action and produces slurry water film, which affects the adhesion force and the play of plough furrow force and causes a different side friction resistance form. Therefore, the pile side friction resistance is mainly divided into three sections, L1, L2, and L3, which are analyzed by the "adhesion-plough" theory, respectively. The distribution of pile side friction force is shown in Figure 6.

The $L1$ section is the upper part of the pile body. In this section, the soil around the pile is repeatedly ploughed by the pile body, leading to the generation of a slurry water film that separates the pile from the soil and to the loss of adhesion force and plough force between the pile and the soil. Consequently, the side friction of the pile is primarily generated by the friction between the slurry water film and the pile body, as shown in Formula (5).

$$F_{L1} = A_{f-p} \tau_f \quad (5)$$

where A_{f-p} is the actual contact unit area between the slurry water film and the pile body; τ_f is the average shear strength of slurry water film.

The *L*2 section is the middle of the pile body. In this section, the ploughing effect of the soil around the pile becomes less, resulting in a thinner slurry water film and the generation of plough force. However, because the presence of the slurry water film prevents the adhesion force from working, the pile side friction resistance is primarily composed of the furrow force between the pile and the soil and the friction between the pile and the slurry water film, as shown in Formula (6).

$$F_{L2} = F_p + F_f = \mu_p W + A_{f-p}\tau_f = \frac{\pi}{2}\cot\beta \cdot W + A_{f-p}\tau_f \quad (6)$$

where F_p is the furrow force; F_f is the friction force between the slurry film and the pile body; μ_p is the furrow friction coefficient; β is the conical half-angle of the hard asperity at the pile–soil interface; W is the positive pressure between pile and soil.

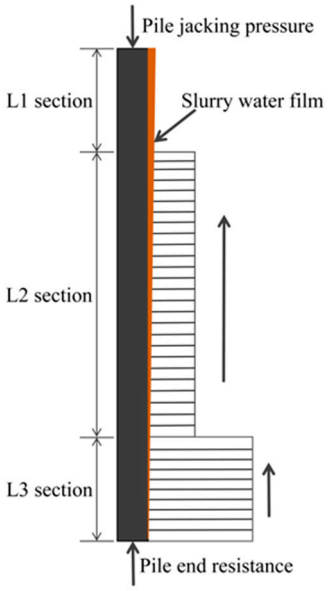

Figure 6. The distribution of pile side friction force.

The *L*3 section represents the lower part of the pile body. In this section, the ploughing effect of the soil around the pile is the weakest. The slurry water film gradually becomes thinner or even disappears. As a result, the adhesion force works, and the ploughing force gradually becomes larger. However, the friction between the slurry water film and the pile body is basically lost, so the pile side friction resistance is mainly influenced by the ploughing force and the adhesion force, as shown in Formula (7).

$$F_{L3} = F_a + F_P = \mu_a W + \mu_P W = \frac{\tau_{S-p}}{H} W + \frac{\pi}{2}\cot\beta \cdot W \quad (7)$$

where F_a is the adhesive force; μ_a is the adhesive friction coefficient; τ_{s-p} is the shear strength of the contact surface between pile and soil; H is the soil hardness.

The relevant parameters of the formula in the above theory are difficult to determine, making it challenging to obtain a quantitative solution. Therefore, this paper primarily utilizes this theory to conduct an effective qualitative analysis of the test results.

3.2. Pile Stress Properties

Figure 7 illustrates the relationship between the applied load on the top of the two test piles and the resistance of the pile side and the pile end. It can be observed from Figure 7 that the overall trend of pile jacking in the two tests is similar. The pile jacking pressure, pile end resistance, and total pile side resistance gradually increase with the depth of

pile jacking. Specifically, the values in test PS2 are higher than those in test PS1. This difference can be attributed to the influence of the static press-in piling machine, which subjects the soil on both sides of the pile to vertical load, causing lateral deformation of the soil. Consequently, during the pile jacking process, additional load is imposed on the pile, leading to an increase in the force between the pile and the soil and to an overall higher value in the test.

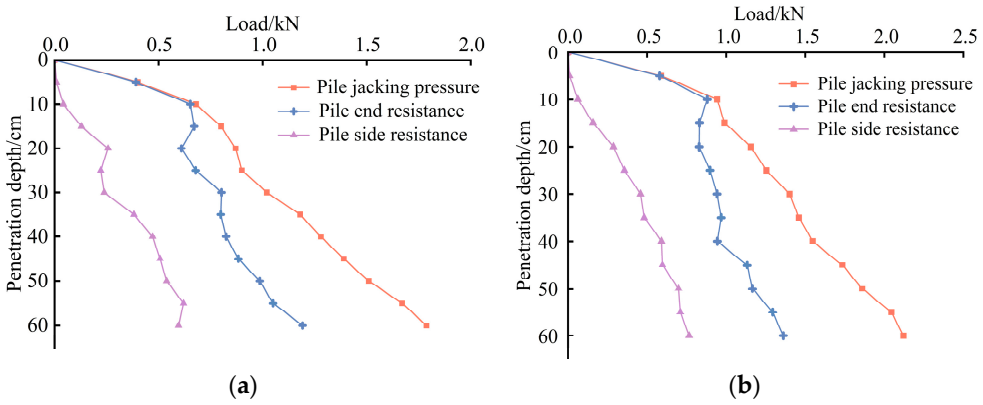

Figure 7. The relationship between pile jacking pressure, pile end resistance, and pile shaft resistance. (**a**) Test PS1. (**b**) Test PS2.

Table 3 presents an analysis of the percentage of pile end resistance and pile side resistance to pile pressure at the end of pile jacking, based on the data obtained from Figure 7.

Table 3. Percentage of pile end resistance and pile side resistance to pile pressure at the end of pile jacking.

Test Number	Pile Jacking Pressure (kN)	Pile End Resistance (kN)	Percentage (%)	Pile Side Resistance (kN)	Percentage (%)
PS1	1.787	1.192	66.7	0.595	33.3
PS2	2.126	1.411	66.3	0.715	33.7

Upon analyzing Table 3, it is evident that the end resistance of the two groups of test piles bears the majority of the load, accounting for more than 50%. Additionally, the total side friction resistance of test PS2 in the table is 0.5% higher than that of the test. This difference can be attributed to the influence of the piling machine, leading to a delayed manifestation of the shaft wall at the pile–soil interface. Additionally, the clay around the pile in PS2 exhibits fewer gaps and strong adhesion with the pile body, which results in a relatively higher total side friction resistance.

3.3. Pile Jacking Resistance

Figure 8 depicts the analysis of pile jacking resistance in the two groups of tests. The pile jacking resistance comprises mainly the pile end resistance and the side friction resistance. Analyzing Figure 8, it is evident that the pile end resistance and pile side resistance in both groups of tests increase with the depth of pile jacking, with the pile end resistance being significantly greater than the pile side resistance. However, when the pile sinking depth is within 10 cm, both tests of piles exhibit a linear increase in end resistance with the growing depth of pile penetration and the total side frictional resistance remains minimal. As the pile sinking depth exceeds 10 cm, the increase rate in end resistance significantly diminished, while the side friction resistance begins to escalate. Moreover, the resistance of the sinking pile in test PS2 is notably greater than that of test PS1 at equivalent sinking depths. Specifically, at the conclusion of the pile driving process, PS2 demonstrated

higher end resistance and side resistance compared to PS1, with margins of 0.219 kN and 0.12 kN, respectively.

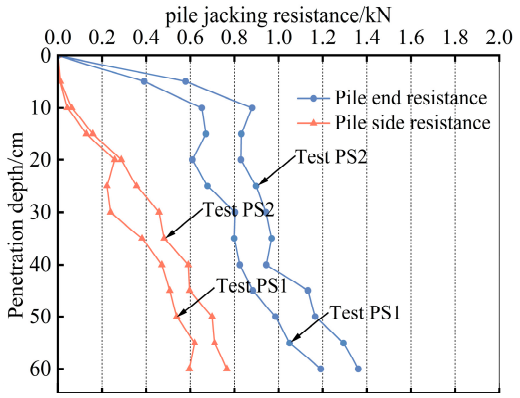

Figure 8. Comparative analysis diagram of pile jacking resistance.

The following is the analysis combined with the "adhesion-plough" theory: in the process of piling jacking, disparate durations of pile ploughing action impact varying depths of the soil, engendering differential degrees of pile–soil separation. The uppermost stratum of soil generates a thicker slurry water film, leading to a discernible attenuation in adhesion. As the soil depth increases, the ploughing action diminishes, which causes thinner slurry water film and a concurrent escalation in pile side resistance. Notably, the top 10 cm of the test soil layer comprises a gravel cushion. Consequently, the pile end resistance in both test groups increases rapidly within the first 10 cm of pile sinking depth, while the total side friction resistance remains minimal. Moreover, the piling machine in PS2 amplifies the lateral pressure of the soil around the pile during the jacking process. As a result, compared to test PS1, the slurry water film between the pile and soil at equivalent soil depths is thinner, leading to increased adhesion points and, subsequently, to higher pile end resistance and side friction resistance.

The discrepancy between the end resistance and the total side friction resistance of the two test piles at each jacking depth is illustrated in Figure 9. Significantly, at a depth of approximately 30 cm, the difference in pile end resistance between the two groups is minimal, while the variance in total side friction resistance is the most significant. Comparatively, with reference to test PS1, the growth rate of the total side friction resistance of test PS2 between 20 and 30 cm of pile depth is accelerated. This can be attributed to the lateral deformation of the soil induced by the static press-in piling machine. However, due to the varying soil depths, the lateral extrusion deformation is not uniform. In this experiment, the influence of the piling machine results in larger lateral extrusion of the soil at 20 to 30 cm, leading to a reduced gap between the pile and the soil and to the ploughing force becoming larger. Thus, the total side friction resistance increases.

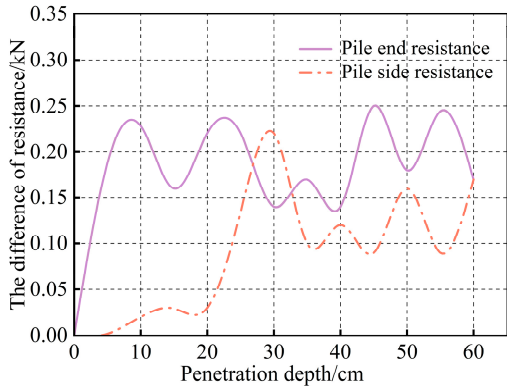

Figure 9. Pile jacking resistance difference curve.

3.4. Pile Shaft Unit Side Friction Resistance

The variation curve of the unit side friction resistance of the pile shaft with respect to the pile penetration depth is depicted in Figure 10. It is evident from the figure that the overall trend of change in the unit side friction resistance of the pile shaft is similar in both test groups. As the pile depth increases, the unit side friction resistance of the pile shaft also increases.

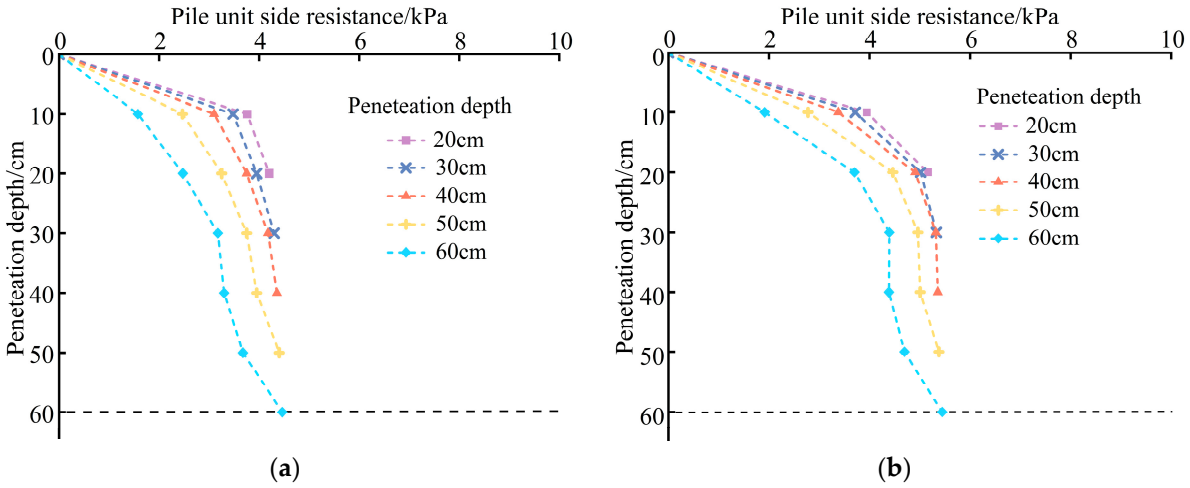

Figure 10. The curve of unit side friction resistance of pile shaft with the depth of pile jacking. (**a**) Test PS1. (**b**) Test PS2.

The analysis of PS1 and PS2 in Figure 10 leads to the conclusion that in the case of test PS2 taking the static press-in piling machine into consideration, the maximum value of unit side friction resistance is 5.44 kPa in PS2, which is obviously larger than that of the 4.46 kPa observed in PS1. It can be attributed to the impact of the pile machine. The soil surrounding the pile experiences lateral squeezing forces, resulting in soil compaction. Therefore, this leads to an increase in the unit side friction resistance of the pile shaft.

The data from the two test groups in Figure 10 illustrate that, at a soil depth of 10 cm, the unit side friction resistance of the pile shaft gradually decreases with an increase in pile depth at the same soil depth, exhibiting a certain regularity. For every 10 cm increase in penetration depth, the reduction value of the unit side friction resistance becomes more significant. This phenomenon, known as "side resistance degradation", has been confirmed by Gavin and Lehane [30] in experiments. Upon the results, it is concluded that as the pile jacking depth increases, the same soil depth experiences repeated ploughing action, leading to the destruction of the adhesion point between the pile and the soil. Simultaneously, the repeated ploughing increases the thickness of the slurry water film between the pile and the soil, ultimately causing a decrease in pile side friction.

Then analyze the trend of the "side resistance degradation" phenomenon as the soil depth varies in Figure 10a,b. Upon normalization of the difference (Δf) between the "side resistance degradation" values Δf_{PS1} obtained from pile test PS1 and Δf_{PS2} obtained from pile test PS2, as illustrated in Figure 11, it is evident that all difference values surpass 0. This indicates that the "side resistance degradation" in test PS1 is more prominent than in test PS2. In other words, the "side resistance degradation" of the unit side friction in test PS2 is generally weakened compared to in test PS1. Furthermore, it can be inferred that as the pile jacking depth increases, Δf gradually decreases. The largest differences in the side resistance degradation occur at depths of 20 cm and 30 cm, signifying that test PS2 exhibits the most significant weakening of "side resistance degradation" at these depths.

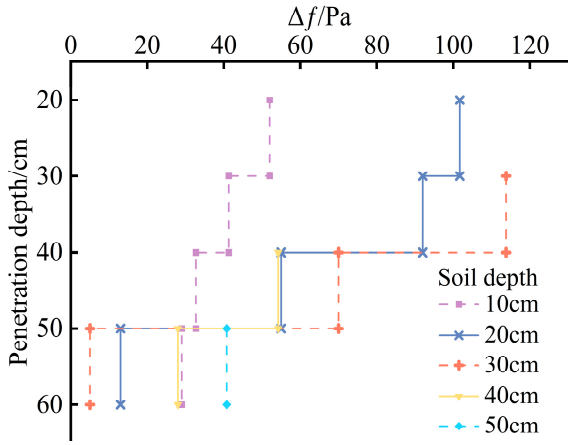

Figure 11. The variation of lateral resistance degradation at different soil depths with the depth of pile jacking.

The analysis of the findings in Figure 11 suggests that the lateral squeezing pressure exerted by the static press-in piling machine on the soil enhances the tightness of the adhesion point between the pile and the soil, thereby increasing the contact firmness between the pile and the soil. As a result, this generally reduces the occurrence of "lateral resistance degradation". Despite the influence of the piling machine, the plough force between pile and soil remains strong as the depth of the pile sinking increases, which results in a reduction in the adhesion point between the upper soil and the pile, as well as a decrease in Δf. This indicates a gradual reduction in the weakening effect of the piling machine on "side resistance degradation". Analysis of the pile sinking resistance reveals significant lateral extrusion at depths of 20 to 30 cm and the maximum Δf at 20 cm and 30 cm caused by the piling machine in this test, which also means the attenuation value of "side resistance degradation" is the highest at these soil depths.

3.5. Pile Shaft Axial Force

Figure 12 depicts the variation curves of axial force with the depth of pile jacking for the two sets of test piles. The diagram reveals that the axial force of the two test piles follows a similar distribution pattern as the pile sinking depth increases. At various depths of pile sinking, the axial force is greatest at the top of the pile and decreases with increasing pile sinking depth. Additionally, the slope of the curve also decreases as the pile sinking depth increases. The reason is that the closer to the pile end, the stronger the adhesive contact between the pile and the soil, so the total side friction resistance of the pile increases along the pile body; therefore, the closer to the pile end, the greater the side friction resistance and the greater the reduction in the axial force of the pile body.

The comparative analysis of the two sets of data in Figure 12a,b reveals that the axial force of the test PS2 pile is generally greater than that of the test PS1 pile. According to Table 4, the axial force of the test PS1 pile decreases from 1.79 kN to 1.19 kN, representing a 34% reduction. Similarly, the axial force of the test PS2 pile decreases from 2.13 kN to 1.36 kN, indicating a 36% decrease in axial force. The decline rate of the axial force for test PS2 is greater than that of test PS1, indicating a larger reduction in axial force for the test PS2 pile compared to the test PS1 pile. This suggests that the side friction resistance of test PS2 is higher. This is primarily due to the consideration of the influence of the static press-in piling machine in test PS2, resulting in a gradual increase in lateral pressure around the pile and a closer bond between the pile body and the soil particles. As a result, a greater level of adhesion is generated compared to in test PS1, leading to increased side friction between the pile and the soil and a weakened performance in axial force transmission.

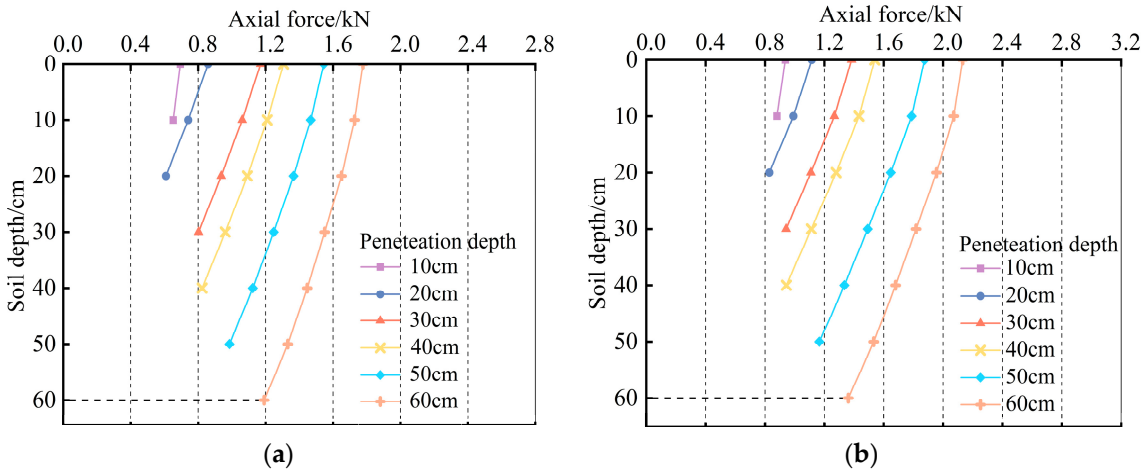

Figure 12. Curve of pile axial force with the change in pile jacking depth. (**a**) Test PS1. (**b**) Test PS2.

Table 4. The decreasing rate of axial force of the pile shaft when the pile sinking depth is 60 cm.

Test Number	Pile Penetration Depth (cm)	Pile Head Axial Force (kN)	Pile End Axial Force (kN)	Axial Force Decline Rate (%)
PS1	60	1.79	1.19	34
PS2	60	2.13	1.36	36

3.6. Soil Pressure around the Pile

Figure 13 depicts the variation curve of soil pressure at different positions throughout the entire process of pile sinking. It can be concluded that as the pile sinking depth increases, the soil pressure is at its highest when the pile end reaches the buried depth of the earth pressure gauge. Subsequently, as the pile jacking depth gradually exceeds the buried depth of the earth pressure gauge, the soil pressure gradually decreases. We analyzed the earth pressure at 1D, 2D, and 3D from the pile shaft at the same buried depth. In test PS1, when the soil depth is 35 cm and the distance from the pile shaft is 1D to 2D and 2D to 3D, the soil pressure around the pile decreases by 4.55 kPa and 8.819 kPa, respectively. Under the same conditions, test PS2 shows a decrease of 3.3 kPa and 13.2 kPa, respectively. Through analysis and comparison, it can be concluded that the decrease in soil pressure is proportional to the distance from the pile shaft. In other words, the farther the distance from the pile shaft, the greater the decrease in soil pressure.

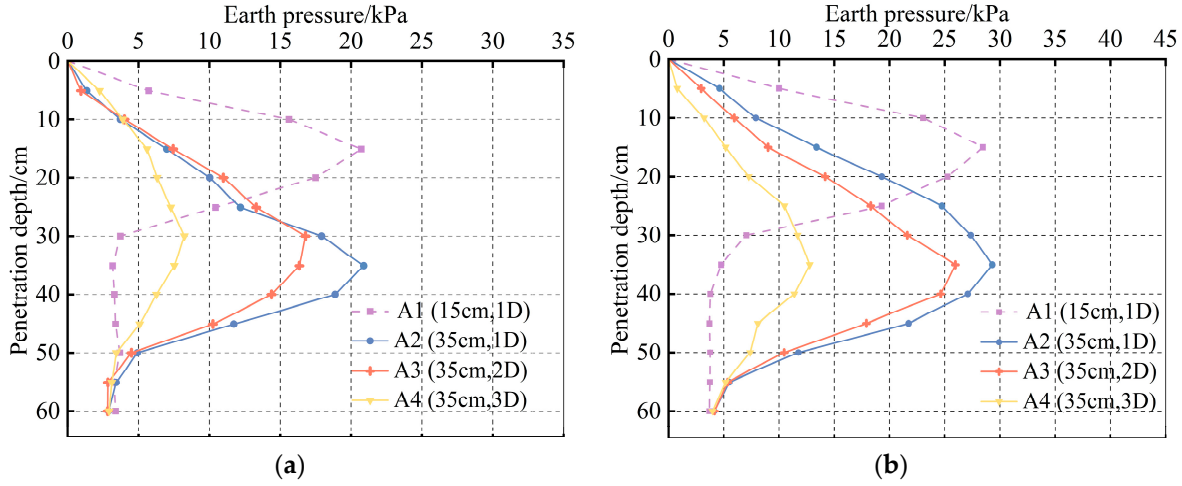

Figure 13. Change curve of soil pressure–pile penetration depth around the pile. (**a**) Test PS1. (**b**) Test PS2.

According to the analysis of Figure 13a,b, it can be observed that when the influence of the static press-in piling machine is considered, the soil pressure around the pile at the same position increases significantly. The reason for this is that the volume of the soil is the same at the same depth of the pile row during the two test pile jacking processes. However, the soil is compacted under the influence of the static press-in piling machine in test PS2, leading to stronger extrusion during the pile sinking process, thus generating greater lateral earth pressure.

4. Conclusions

In contrast to the conventional model test exclusively addressing a jacked pile, the inclusion of a static press-in piling machine has an influence on the process of pile jacking, and it is more in line with engineering practice. Through comparative analysis of the data, the following conclusions can be drawn:

(1) The overall distribution law of the stress characteristics of the pile during the pile jacking process is basically the same. However, under the effect of the static press-in piling machine, the results are different from the conventional model test. When compared with the test that only considers the pile, the pile pressing force, the pile end resistance, and the total side friction resistance of the pile are relatively high. Additionally, the proportion of the total side friction resistance to the pile pressing force increases when the piling machine is considered.

(2) The pile jacking resistance is also affected by the static press-in piling machine. Under the influence of the piling machine, the pile end resistance and the pile side resistance have been increased to varying degrees. Although it is uneven, the growth rate of the total side friction resistance is accelerated when the pile sinking depth is 20 to 30 cm.

(3) The distribution trend of the axial force of the two piles is also basically the same. When considering the influence of the static press-in piling machine, the axial force of the pile exhibits an increasing trend in conjunction with its decreasing rate.

(4) When analyzing the influence of the static press-in piling machine on the unit side friction resistance of the pile body, it is found that the resistance relatively increases when the piling machine is considered. However, the phenomenon of "side resistance degradation" decreases. The reduction in "side resistance degradation" is the greatest at a depth of 20 cm to 30 cm, and this reduction gradually diminishes with increasing soil depth.

(5) The soil pressure around the pile generally increases first and then decreases. When the pile sinking depth reaches the buried depth of the soil pressure gauge, the soil pressure value is the largest. The farther away from the pile, the smaller the earth pressure, showing a linear decreasing trend. At the same time, the soil pressure around the pile also increases when the static press-in piling machine is considered.

(6) According to the theory of "adhesion-plough" proposed from the perspective of tribology, it can effectively explain the reasons for the change in experimental data under the action of a static press-in piling machine compared to the static pressure single pile and provide a theoretical basis for the test data.

The analysis of the above shows the impact of the static press-in piling machine on the pile jacking, emphasizing the importance of selecting a suitable piling machine model in practical applications. This will enhance the accuracy of estimating pile jacking resistance prior to construction and assist in establishing a better understanding of the coupling mechanism between the piling machine and the quality of pile jacking in practical applications.

Future research can also involve conducting jacked pile model box tests to investigate soil compaction effects while considering the impact of the piling machine. By utilizing numerical simulations and field tests, the influence of various combinations of pile machine models, pile types, and soil layers on penetration characteristics and soil compaction effects can be analyzed. Furthermore, the research findings on jacked piles can be extended to other pile installation methods, such as bored piles and static drilling root piles, in order

to establish a comprehensive theory on the collaborative fusion of piling machine, piles, and site soil layers. This will further strengthen the interdisciplinary collaboration between civil and mechanical disciplines, enhancing the applicability and scope of the research.

Author Contributions: Conceptualization, Y.L. and R.Z.; methodology, R.Z.; validation, R.Z., Y.D. and Y.L.; formal analysis, R.Z. and Y.L.; investigation, Y.D.; resources, R.Z.; data curation, Y.L.; writing—original draft preparation, Y.L.; writing—review and editing, R.Z. and Y.D.; visualization, Y.L.; supervision, Y.D.; project administration, R.Z.; funding acquisition, R.Z. All authors have read and agreed to the published version of the manuscript.

Funding: This research was funded by low-carbon ultra-high-strength prefabricated pile products and green non-squeezed soil construction key technology research and demonstration-green non-squeezed soil construction equipment development and construction environmental effects research, Ningbo major scientific and technological task research project, grant number 20212ZDYF020038, and the Beilun District Key Core Technology Research Project: 'Key Technology Research and Development and Industrialization of Intelligent Pile Drilling Mixer', grant number 2022001.

Institutional Review Board Statement: Not applicable.

Informed Consent Statement: Not applicable.

Data Availability Statement: The data used to support the findings of this study are currently under embargo while the research findings are commercialized. Requests for data, 12 months after publication of this article, will be considered by the corresponding author.

Conflicts of Interest: The authors declare no conflicts of interest.

References

1. Zhang, L.M.; Wang, H. Field study of construction effects in jacked and driven steel H-piles. *Géotechnique* **2009**, *59*, 63–69. [CrossRef]
2. Yang, J.; Tham, L.G.; Lee, P.K.K.; Chan, S.T.; Yu, F. Behaviour of jacked and driven piles in sandy soil. *Géotechnique* **2006**, *56*, 245–259. [CrossRef]
3. Wang, Z.; Miao, L.; Wang, F. Theoretical and numerical analysis of jacked pile in sand. In Proceedings of the 2012 GeoCongress, State of the Art and Practice in Geotechnical Engineering, Oakland, CA, USA, 25–29 March 2012; pp. 245–254.
4. Goncharov, B.V.; Karev, V.M.; Troyanovskii, Y.V. Results of comparative tests of mobile machines for driving piles. *Soil Mech. Found. Eng.* **1964**, *1*, 36–39. [CrossRef]
5. Eskişar, T.; Akboğa Kale, Ö. Evaluation of pile driving accidents in geotechnical engineering. *Int. J. Occup. Saf. Ergon.* **2022**, *28*, 625–634. [CrossRef] [PubMed]
6. Doherty, P.; Gavin, K. Shaft capacity of open-ended piles in clay. *J. Geotech. Geoenviron. Eng.* **2011**, *137*, 1090–1102. [CrossRef]
7. Kou, H.L.; Yu, F.; Liu, T. Strain monitoring on PHC pipe piles based on fiber bragg grating sensors. *J. Perform. Constr. Facil.* **2019**, *33*, 04019003. [CrossRef]
8. Wang, Y.; Sang, S.; Zhang, M.; Liu, X.; Yang, S. Field test of earth pressure at pile-soil interface by single pile penetration in silty soil and silty clay. *Soil Dyn. Earthq. Eng.* **2021**, *145*, 106666. [CrossRef]
9. Wang, Y.; Sang, S.; Zhang, M.; Bai, X.; Su, L. Investigation on in-situ test of penetration characteristics of open and closed PHC pipe piles. *Soils Found.* **2021**, *61*, 960–973. [CrossRef]
10. Paik, K.; Salgado, R.; Lee, J.; Kim, B. Behavior of open-and closed-ended piles driven into sands. *J. Geotech. Geoenviron. Eng.* **2003**, *129*, 296–306. [CrossRef]
11. Ding, X.; Shi, Y.; Chen, R.; Zhou, M. Friction anlysis of large diameter steel cylinder penetration process using 3D-DEM. *Granul. Matter* **2021**, *23*, 24. [CrossRef]
12. Jin, Y.F.; Yin, Z.Y.; Wu, Z.X.; Daouadji, A. Numerical modeling of pile penetration in silica sands considering the effect of grain breakage. *Finite Elem. Anal. Des.* **2018**, *144*, 15–29. [CrossRef]
13. Zhou, J.; Jian, Q.W.; Zhang, J.; Guo, J.J. Coupled 3D discrete-continuum numerical modeling of pile penetration in sand. *J. Zhejiang Univ. Sci. A* **2012**, *13*, 44–55. [CrossRef]
14. Zhang, M.Y.; Deng, A.F.; Gan, T.J. Displacement penetration method used for numerical simulation to jacked pile. *Rock Soil Mech.* **2003**, *24*, 113–117.
15. Abendroth, R.E.; Greimann, L.F. Pile behavior established from model tests. *J. Geotech. Eng.* **1990**, *116*, 571–587. [CrossRef]
16. Altaee, A.; Fellenius, B.H.; Evgin, E. Load transfer for piles in sand and the critical depth. *Can. Geotech. J.* **1993**, *30*, 455–463. [CrossRef]
17. Lehane, B.M.; Gavin, K.G. Base resistance of jacked pipe piles in sand. *J. Geotech. Geoenviron. Eng.* **2001**, *127*, 473–480. [CrossRef]
18. Gong, W.; Li, J.; Li, L.; Zhang, S. Evolution of mechanical properties of soils subsequent to a pile jacked in natural saturated clays. *Ocean Eng.* **2017**, *136*, 209–217. [CrossRef]

19. Zhang, Y.; Wang, Y.; Liu, X.; Sang, S. Research of jacked pile penetration test based on airbag loading. *Soil Dyn. Earthq. Eng.* **2023**, *164*, 107407. [CrossRef]
20. Wang, Y.Y.; Sang, S.K.; Zhang, M.Y.; Jeng, D.S.; Yuan, B.X.; Chen, Z.X. Laboratory study on pile jacking resistance of jacked pile. *Soil Dyn. Earthq. Eng.* **2022**, *154*, 107070. [CrossRef]
21. Wang, Y.; Sang, S.; Liu, X.; Huang, Y.; Zhang, M.; Miao, D. Model test of jacked pile penetration process considering influence of pile diameter. *Front. Phys.* **2021**, *9*, 616410. [CrossRef]
22. Wang, Y.; Wang, X.; Li, S.; Wang, J.; Zhang, C.; Li, Y. Field testing study on jacked pile penetration characteristics in laminated clay based on FBG sensing technology. *Soil Dyn. Earthq. Eng.* **2023**, *168*, 107848. [CrossRef]
23. Lu, Q.; Gong, X.; Ma, M. Squeezing effects of jacked pile considering static pile press machine's action. *J. Zhejiang Univ. Eng. Sci.* **2007**, *41*, 1132.
24. Wang, H.; Wei, D.D. Numerical simulation research of the effect of squeezing soil due to pile driven in soft clay restrained on surface. *Rock Soil Mech.* **2002**, *23*, 107–110.
25. Toma, S.; Seto, K.; Chen, W.F. Comparisons of Static and Dynamic Analyses on Toppling Behaviors of Pile Driving Machinery, etc., on Soft Foundation. *Arch. Adv. Eng. Sci.* **2023**, 1–15. [CrossRef]
26. *GB/T 50123-2019*; Geotechnical Test Method Standards. People's Republic of China Industry Standards Writing Group: Beijing, China, 2019.
27. Hu, Y.Q.; Tang, L.S.; Li, Z.Y. Mechanism of sliding friction at pile-soil interface of jacked pile. *Rock Soil Mech.* **2015**, *36*, 1288–1294.
28. Komvopoulos, K.; Saka, N.; Suh, N.P. The mechanism of friction in boundary lubrication. *J. Tribol.* **1985**, *107*, 452–462. [CrossRef]
29. Zeng, Z.; Wang, L.; Chen, L.; Zhang, J. The correlation between the hardness and tribological behaviour of electroplated chromium coatings sliding against ceramic and steel counterparts. *Surf. Coat. Technol.* **2006**, *201*, 2282–2288. [CrossRef]
30. Gavin, K.G.; Lehane, B.M. The shaft capacity of pipe piles in sand. *Can. Geotech. J.* **2003**, *40*, 36–45. [CrossRef]